

Self-assembled hexagonal double fishnets as negative index materials

Kristof Lodewijks,^{1,2,a)} Niels Verellen,^{1,2,3} Willem Van Roy,¹ Victor Moshchalkov,³ Gustaaf Borghs,^{1,3} and Pol Van Dorpe¹

¹IMEC, Kapeldreef 75, B-3001 Leuven, Belgium

²Department of Electrical Engineering (ESAT), KU Leuven, Kasteelpark Arenberg 10, B-3001 Leuven, Belgium

³INPAC Institute for nanoscale Physics and Chemistry, KU Leuven, Celestijnenlaan 200 D, B-3001 Leuven, Belgium

(Received 9 November 2010; accepted 2 February 2011; published online 28 February 2011)

We show experimentally the use of nanosphere lithography for fabricating negative index metamaterials in the near-infrared wavelength range. We investigated a specific implementation of the widely studied double fishnet metamaterials, consisting of a gold-silica-gold layer stack perforated by a hexagonal array of round holes. Tuning of the hole diameter allows to tailor these self-assembled materials as single- or double negative metamaterials. © 2011 American Institute of Physics. [doi:10.1063/1.3560444]

Since the introduction of negative index materials (NIMs) by Veselago¹ and the discovery of the possibility of realizing subwavelength resolution for imaging devices based on these metamaterials by Pendry,² many different designs have been proposed to make the “perfect lens” dream reality. A widely studied geometry in the visible and near-infrared (NIR) wavelength range is the double fishnet (DFN) structure,^{3–7} which consists of a stack of metal-insulator-metal (MIM) layers perforated by a periodic array of holes. The pioneering work by Dolling *et al.*⁴ demonstrated the reversal of the phase velocity, and more recently, also negative refraction was observed in a multilayer fishnet prism structure.⁸ The behavior of these NIMs is governed by a magnetic resonance that is excited in the MIM cavities in between the holes and the negative permittivity (ϵ) of the metal layers.⁹ At the magnetic resonance, plasmons are excited on the top- and bottom interface of the insulator layer of the MIM cavities, which give rise to a strong magnetic dipole resonance that lowers the effective permeability (μ) which can even reach negative values. Simultaneously negative values for ϵ and μ give rise to a negative value for the refractive index (n). Based on the real parts ($'$) of the effective parameters of the metamaterial, NIMs can be classified as single-NIMs or double NIMs (SN-NIMs with $\epsilon' < 0$ and $\mu' > 0$ while $n' < 0$ and DN-NIMs with $\epsilon' < 0$ and $\mu' < 0$ while $n' < 0$). The figure of merit (FOM) for NIMs is defined as the amplitude ratio between the real ($'$) and imaginary ($''$) part of n ($\text{FOM} = |n' / n''|$). Depending on the SN or DN nature of the NIM, low (SN) or high (DN) values of the FOM are observed. A major drawback of most structures reported to date is that the fabrication involves expensive and low-throughput lithography steps such as e-beam lithography (EBL) or focused ion beam milling, which limits the potential usage of these metamaterials in large-scale applications.

Here we show that we can circumvent this limitation by using nanosphere lithography (NSL), which allows to create large-area DFN metamaterials consisting of a MIM layer stack perforated by a hexagonal array of holes. The hole

pattern is generated using a self-assembled close packed monolayer of 550 nm polystyrene (PS) beads. The pitch of the holes can be tuned by the bead size, while their diameter can be tuned by the bead shrinking step, which allows us to create both SN- and DN-NIMs. Moreover, our fabrication procedure based on ion beam etching (IBE) enables an increase in the overall layer thickness of the NIM, which paves the way to multiple functional layers. The sample geometry is illustrated in (Fig. 1). The structure consists of a Au–SiO₂–Au MIM stack (60–60–60 nm) perforated with a hexagonal array of round holes on top of a glass substrate.

The samples were fabricated by NSL using 550 nm PS beads. The MIM layers are sputtered onto the glass substrate and subsequently covered with MET-2D (Ref. 10) resist. The resist layer is covered with a 10 nm Au protection layer by sputtering. On top of these layers, a hexagonal close-packed monolayer of PS beads is deposited by spincoating, yielding particle arrays up to $100 \times 100 \mu\text{m}^2$ that have a single lattice orientation and a small number of defects. The PS beads are

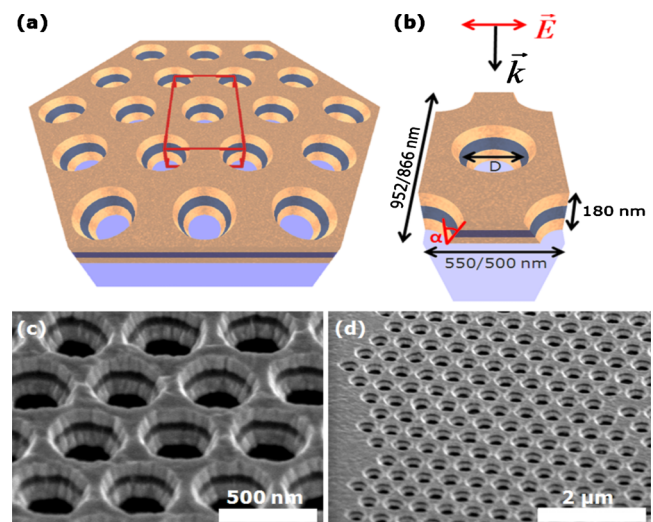


FIG. 1. (Color online) (a) Schematic sample structure. (b) Unit cell for simulations (dimensions for the NSL/EBL samples), D is the diameter and α the 20° sidewall angle of the holes. Detailed scanning electron microscope picture of the NSL sample (c) and a perfectly ordered domain with some defects (d).

^{a)}Author to whom correspondence should be addressed. Electronic mail: kristof.lodewijks@imec.be.

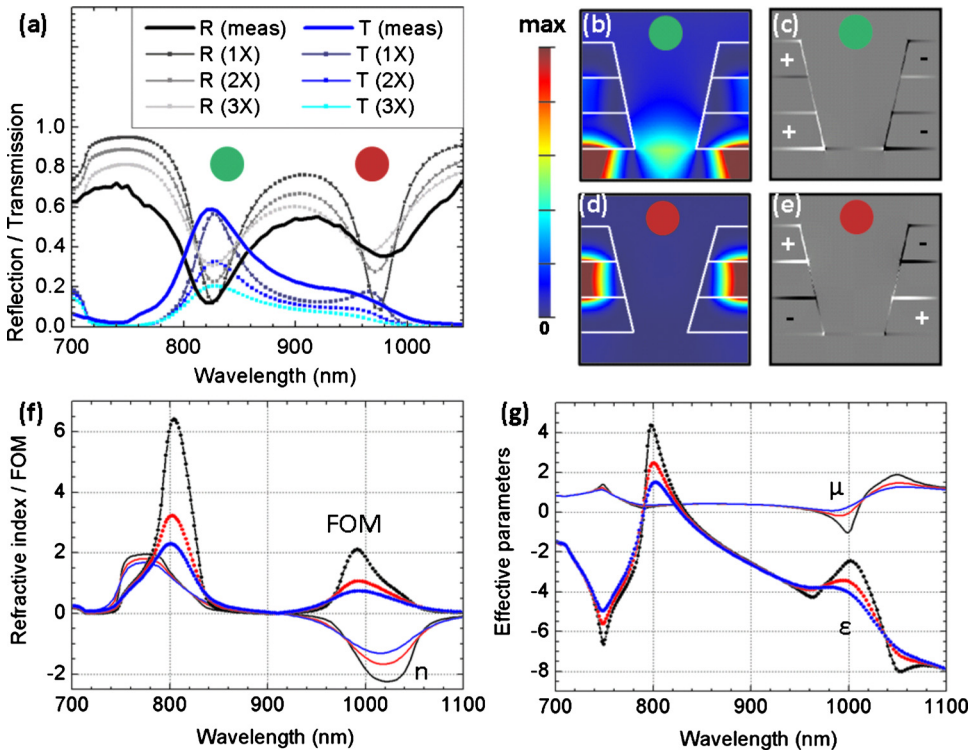


FIG. 2. (Color online) Measurements and simulations for a self-assembled hexagonal DFN. (a) Measured (full lines) and simulated (dotted lines) reflection and transmission spectra with different damping. (1, 2, 3X = number of times the bulk imaginary ϵ of Au). (b) and (d) show the magnetic field intensity plot at the 825 nm and 980 nm resonance, respectively. (c) and (e) show the charge density plot at the 825 nm and 980 nm resonance, respectively. (f) Simulated real part of n and the FOM for different damping in the Au layers. (g) Simulated effective parameters: ϵ' and μ' for different damping in the Au layers.

fixed on the substrate by a short annealing step and subsequently the beads are shrunk using O_2 -plasma etching. In this step the Au protection layer prevents etching of the resist layer. The PS beads serve as a template for the hole array, when we cover them by evaporation with a 5 nm Ti layer, followed by a lift-off of the beads in toluene. The hole pattern is transferred into the Au protection layer by IBE and into the resist layer by O_2 -plasma etching. Next the pattern is transferred from the resist into the MIM by IBE [introducing a sidewall angle, see Fig. 1(b)], while the remaining resist is removed using an O_2 -plasma etch. For reference purposes we made samples by EBL. The NSL step is replaced by e-beam exposure (without sacrificial Au layer) and development of the MET-2D resist. The hole pattern is etched into the MIM stack by IBE and the remaining resist is removed using O_2 -plasma etching.

The optical response of our samples was modeled using finite-difference time domain simulations.¹¹ A rectangular unit cell with periodic boundary conditions was used [Figs. 1(a) and 1(b)]. The complex fields on the top and bottom surface of the MIM trilayer structure were averaged over the unit cell (homogenization) in order to extract the effective material parameters,¹² taking into account the bianisotropy (sidewall angle of holes) of the samples. In that way, the complex effective parameters (n , Z , ϵ , and μ) and the FOM were calculated (for details see Ref. 13). While this method is often debated in literature, we believe that for the case of perpendicular incidence, the bianisotropy correction in the propagation direction is sufficient to qualitatively describe the behavior of these NIMs.

An overview of the optical response of the self-assembled hexagonal DFN with a hole diameter of 270 nm and a pitch of 550 nm is given in Fig. 2. The measured and simulated transmission and reflection data [Fig. 2(a)] show two pronounced resonances which exhibit good qualitative agreement. The corresponding magnetic field intensity plots [Figs. 2(b) and 2(d)] and charge density plots [Figs. 2(c) and

2(e)] provide good insight in the nature of these modes. The magnetic field intensity plots show the out-of-plane field component in a cross section of the MIM layer stack. This perpendicular component is a good measure for the excitation of surface plasmons, and illustrates how the first mode at 825 nm [Fig. 2(b)] is confined at the interface between the bottom Au layer and the substrate, while the second mode at 980 nm [Fig. 2(d)] is confined on the top and bottom interfaces of the SiO_2 layer. The corresponding charge density plots show that for the first mode [Fig. 2(c)] parallel and for the second mode [Fig. 2(e)] antiparallel displacement currents are excited in the Au layers of the MIM cavity. The second mode clearly shows a strong magnetic resonance [Fig. 2(d)] where an out-of-phase magnetic dipole (with respect to the incident plane wave) is excited in the SiO_2 of the MIM cavity, and that gives rise to a strong decrease in the effective μ' of the metamaterial. In combination with the negative ϵ' of the Au layers, this results in a negative value for n' . The effective material parameters extracted from simulations are summarized in [Figs. 2(f) and 2(g)]. We first carried out the extraction with the bulk properties of Au (Ref. 14) and then gradually increased the ϵ'' (up to three times the bulk value), to compensate for fabrication imperfections and interface roughness. When increasing ϵ'' of the Au layers, all resonances are damped (decreased amplitude) and broadened while maintaining their spectral position. This damping is also reflected in the extracted effective parameters, which show a decrease in the resonance amplitude as ϵ'' of the Au layers is increased. Smaller absolute values for n' and larger values for n'' are obtained, resulting in a decrease in the FOM [Fig. 2(f)]. The resonances in the effective ϵ' and μ' , are also decreased in amplitude [Fig. 2(g)]. When comparing the measured spectra with simulation data, we clearly observe that for the first resonance, the bulk damping coefficients give us the best fit, which can be explained by its nature. The mode is dominated by the bottom hole cavity and plasmons excited at the interface between the substrate and

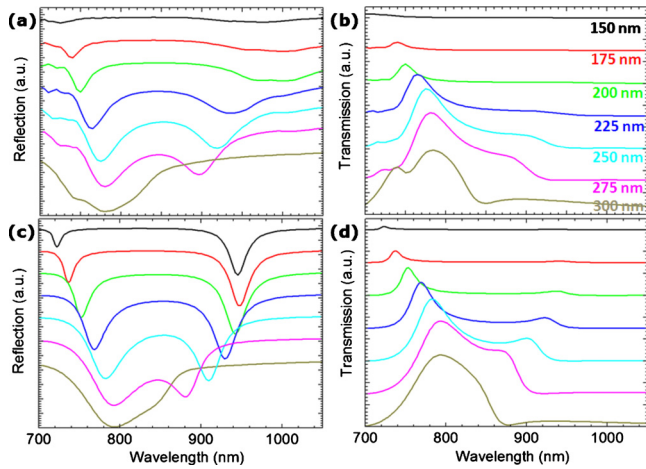


FIG. 3. (Color online) Reflection and transmission spectra for EBL based hexagonal DFNs with $150 \text{ nm} \leq D \leq 300 \text{ nm}$. Measured reflection (a) and transmission (b). Simulated reflection (c) and transmission (d).

the bottom Au layer [Fig. 2(b)]. Since the substrate roughness is much smaller than the roughness of the sputtered MIM layers, we do not expect much additional damping on top of the bulk material properties.¹⁵ For the magnetic resonance on the other hand, we see more damping in the measurement than for the simulation with the bulk Au parameters (1X). When increasing ϵ'' (2X and 3X) in the simulations, we clearly see the modes becoming less pronounced, which is most apparent in the transmission spectrum near the magnetic resonance. The steplike behavior is observed in all simulations but the sharp edge that is observed for the bulk ϵ'' becomes less steep as the damping is increased. Therefore, the steplike behavior in the transmission spectrum is a good measure to determine the importance of damping, by fitting the measured spectrum to the simulated spectra with different values of the ϵ'' . In practice, we search for qualitative correspondence of the shape of the magnetic resonance to determine the most appropriate damping. Based on experimental results for various hole sizes, we suggest that doubling the ϵ'' of the Au layers is sufficient to account for the increased damping due to surface roughness and the nanoscale dimensions of the metamaterial. Again, the increased damping can be understood from the nature of the resonance. At the magnetic resonance, plasmons are excited on the top and bottom of the SiO_2 spacer, which are more prone to surface roughness, as these are created by sputtering.¹⁵

Figure 3 shows an overview of the measured and simulated transmission and reflection spectra for a batch of hexagonal DFNs, fabricated by EBL, with $150 \text{ nm} \leq D \leq 300 \text{ nm}$ and a pitch of 500 nm. The measured spectra show good agreement to the simulated spectra, in which bulk material parameters were used. For all samples, the two main modes of the structure can be clearly observed, and show the expected wavelength shifts with respect to the diameter. The first resonance between 750 and 800 nm shows a redshift with increasing diameter, which is related to the cut-off of the hole transmission. As the hole size is decreased, the resulting decrease in transmission is smaller for shorter than for longer wavelengths, due to the nonlinear dependence of

the transmission beyond the cut-off frequency of the hole waveguide.¹⁶ The second mode between 900 and 950 nm shows a blueshift with increasing diameter. As this mode is related to the excitation of plasmons⁹ on the interfaces of the SiO_2 layer, the blueshift with increasing diameter can be attributed to decreasing MIM cavity length.

All samples shown in Fig. 3 exhibit negative values for n' around the magnetic resonance. The strength of the magnetic resonance is different for the various hole sizes, and the strongest resonance is observed for a diameter of 250 nm, which is the only sample that exhibits DN behavior (using double ϵ'').

When we compare the measured spectra for NSL samples [Fig. 2(a)] and EBL samples [Figs. 3(a) and 3(b)], we observe some minor differences. Both sample types show broadening of the measured resonances with respect to the simulated spectra, but the broadening is more pronounced for NSL samples (Q-factor of about 15 versus 20 for EBL). This can be attributed to line defects and missing holes, but also to size variations in the PS beads and imperfect hole shapes due to the shrinking step.

To summarize, we have shown the feasibility to use NSL for the fabrication of large area metamaterials that exhibit a negative value of the refractive index in the NIR wavelength range. Depending on the hole diameter, the metamaterials can be tuned to be SN or DN in nature. Moreover, we have shown that the damping of the resonances due to the nanoscale structure and fabrication imperfections seems to be smaller compared to earlier works, and should in our case only be taken twice as large as the bulk permittivity for Au in order to allow extraction of effective material parameters.

The authors acknowledge financial support from IWT, FWO, and Methusalem funding (Flemish Government).

¹V. G. Veselago, *Sov. Phys. Usp.* **10**, 509 (1968).

²J. B. Pendry, *Phys. Rev. Lett.* **85**, 3966 (2000).

³G. Dolling, C. Enkrich, M. Wegener, C. M. Soukoulis, and S. Linden, *Opt. Lett.* **31**, 1800 (2006).

⁴G. Dolling, C. Enkrich, M. Wegener, C. M. Soukoulis, and S. Linden, *Science* **312**, 892 (2006).

⁵G. Dolling, M. Wegener, C. M. Soukoulis, and S. Linden, *Opt. Lett.* **32**, 53 (2007).

⁶U. K. Chettiar, A. V. Kildishev, H.-K. Yuan, W. Cai, S. Xiao, V. P. Drachev, and V. M. Shalaev, *Opt. Lett.* **32**, 1671 (2007).

⁷S. Xiao, U. K. Chettiar, A. V. Kildishev, V. P. Drachev, and V. M. Shalaev, *Opt. Lett.* **34**, 3478 (2009).

⁸J. Valentine, S. Zhang, T. Zentgraf, E. Ulin-Avila, D. A. Genov, G. Bartal, and X. Zhang, *Nature (London)* **455**, 376 (2008).

⁹A. Mary, S. G. Rodrigo, F. J. Garcia-Vidal, and L. Martin-Moreno, *Phys. Rev. Lett.* **101**, 103902 (2008).

¹⁰XP-5271 (A-ZZ) Positive NGL Photoresist, Dow Corning Corporation, www.dowcorning.com.

¹¹FDTD Lumerical, Lumerical Solutions Inc., www.lumerical.com/fdtd.

¹²D. R. Smith, D. C. Vier, T. Koschny, and C. M. Soukoulis, *Phys. Rev. E* **71**, 036617 (2005).

¹³See supplementary material at <http://dx.doi.org/10.1063/1.3560444> for details on sample fabrication and simulations.

¹⁴P. B. Johnson and R. W. Christy, *Phys. Rev. B* **6**, 4370 (1972).

¹⁵P. Nagpal, N. C. Lindquist, S.-H. Oh, and D. J. Norris, *Science* **325**, 594 (2009).

¹⁶K. L. van der Molen, F. B. Segerink, N. F. van Hulst, and L. Kuipers, *Appl. Phys. Lett.* **85**, 4316 (2004).